TRANSACTIONS OF THE INSTITUTE OF AVIATION eISSN 2300-5408
No. 1(238), pp. 70-90, Warsaw 2015

PATTERN OF HELICOPTER ROTOR LOADS AND BLADE DEFORMATIONS IN SOME STATES OF FLIGHT ENVELOPE

JAROSŁAW STANISŁAWSKI

New Technology Center, Aircraft Design Department, Institute of Aviation, al. Krakowska 110/114, 02-256 Warsaw, Poland, stanjar@ilot.edu.pl

Abstract

Paper contains a calculated range of helicopter rotor loads and deformations of the rotor blades which can occur within the flight envelope in different states: hover, level flight, autorotation, pull-up. The rotor loads were determined by using a computer simulating program including the model of the deformable rotor blade. The equations of motion of the rotor blade were solved by applying Galerkin's method. The results of calculations were presented in the form of plots showing time-run of the loads and the distributions of deformations due to the blade azimuth position on the rotor disk.

Keywords: helicopter, rotor, blade.

INTRODUCTION

The rotor is the main element of a helicopter structure providing lift and horizontal components of thrust, and also moments for a longitudinal and lateral control. Realization of flights at a large scope of velocity ranging from hover to high speed flight exceeding 300 km/h requires the control of the rotor blades including collective and cyclic pitch angles, which is accomplished by swashplate position and its displacements.

A flight with the whirling rotor generates variable conditions of the airflow around blade sections including changes of distribution of the local air speed and an angle of attack during a rotor revolution. The large airflow changes of blade cross-sections are the result of summation of rotational rotor speed and helicopter forward speed. The local attack angle depends on the localization of cross-section along the rotor blade, pitching blade due to control, blade flapping and torsion deformation of the blade.

The knowledge of the level of variable loads acting on the rotor and the size of the generated blade deflections is necessary to design helicopters and to define the conditions of their safe operation. A determination of blade deflections and the rotor loads can be fulfilled in a process of calculation by applying a computer program. The presented results of simulating computation were obtained by using a modified version of an in-house developed computer program [1], [2].

MODEL OF HELICOPTER ROTOR

The helicopter rotor is treated as a set of elastic axes with inertial features corresponding to a mass distribution of a real blade and stiffness distribution for torsion and bending in a flap and chord plane. The inertial features of the blade, divided into segments, are represented by a system of lumped masses connected to the elastic axis (Fig. 1). The articulations of the rotor head are modelled by additional degrees of freedom for angular motion at the cross-section corresponding to the position of axial, lagging and flapping joints.

The calculation algorithm implements multi-blade analysis where the loads and deflections are determined for blades located at a different azimuth on the rotor plane. The resultant loads of the rotor shaft at a given moment are obtained after summing the reaction of all blades. The physical model of the blade was defined by applying following assumptions:

- continuous mass distribution of the real blade was replaced by lumped masses located at the centers of gravity of blade segments,
- cross-sections of the blade with concentrated masses are connected by segments of elastic axis with constant stiffness,
- elastic axis undergoes torsion and bending in thrust and revolution planes,
- the lumped masses represent the inertial features (mass m_i and inertial moments I_{xi}, I_{yi}, I_{zi}) of corresponding blade segments,
- the blade is connected with the rotor head by articulated joints,
- the flap and pitch coupling of the blade motion is included,
- the ideal stiffness of the rotor shaft is assumed,
- in non-deformed state the elastic axis takes position of blade pitch axis.

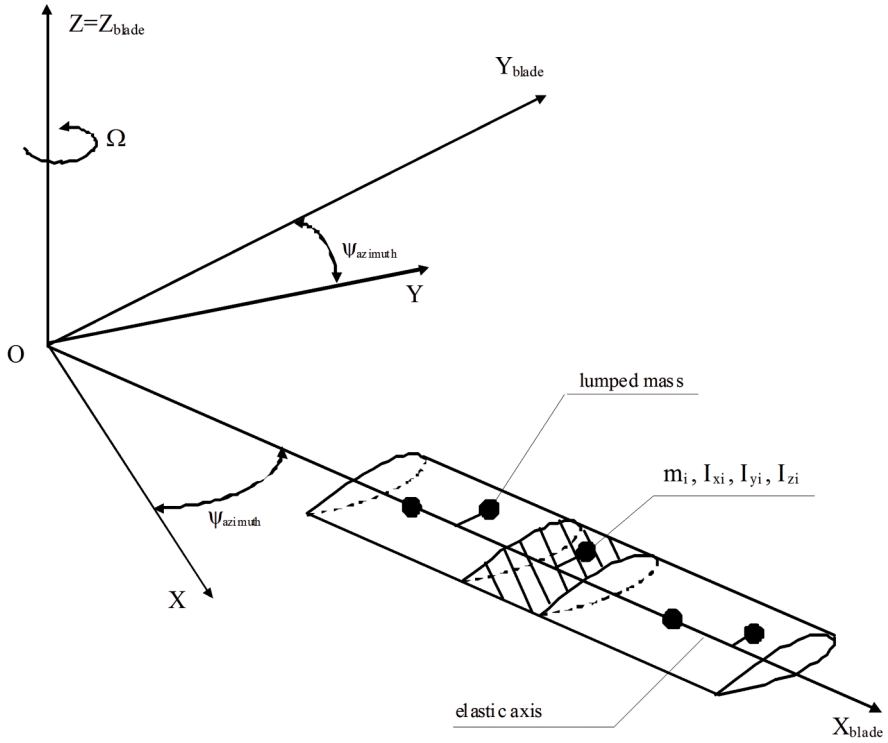

Fig. 1. Physical model of rotor blade – elastic axis with set of lumped masses [J. Stanisławski, 2014]

The equations of motion of rotating elastic axis form the mathematical model of the rotor blade. For continuous distribution of mass and stiffness the equations of motion are as follows:

- for in-plane bending

$$\int_0^R m(x)\ddot{y}\,dx+\int_0^R\left\{\frac{d^2}{dx^2}\left[EJ_Z\left(\frac{d^2y}{dx^2}\right)\right]-\frac{d}{dx}\left(N\frac{dy}{dx}\right)+m(x)\omega^2 y\right\}dx=\int_0^R\left(F_{Y_{EXT}}-F_{Y_{IN}}\right)dx \tag{1}$$

- for out-of-plane bending

$$\int_0^R m(x)\ddot{z}\,dx+\int_0^R\left\{\frac{d^2}{dx^2}\left[EJ_Y\left(\frac{d^2z}{dx^2}\right)\right]-\frac{d}{dx}\left(N\frac{dz}{dx}\right)\right\}dx=\int_0^R\left(F_{Z_{EXT}}-F_{Z_{IN}}\right)dx \tag{2}$$

- for torsion

$$\int_0^R I_X(x)\ddot{\varphi}\,dx+\int_0^R\frac{d}{dx}\left[GJ_X\left(\frac{d\varphi}{dx}\right)\right]dx=\int_0^R\left(M_{S_{EXT}}(x)-M_{S_{IN}}(x)\right)dx, \tag{3}$$

where

$F_{Y_{EXT}}, F_{Z_{EXT}}, M_{S_{EXT}}$ – shear forces and torsion moment of external load acting on segment *dx* of elastic axis,

$F_{Y_{IN}}, F_{Z_{IN}}, M_{S_{IN}}$ – inertial forces and torsion moment of inertial forces respectively reduced by following components $m\ddot{y}, m\ddot{z}, I_X\ddot{\varphi}$ acting on segment *dx* of elastic axis.

The bending and torsion moments acting at the cross-section of the blade are defined by relations:

$$M_Y=EJ_Y\frac{d^2z}{dx^2},\ M_Z=EJ_Z\frac{d^2y}{dx^2},\ M_S=GJ_X\frac{d\varphi}{dx}.$$

In the case of a rotating blade the equations of motion must include the effects of centrifugal forces. The centrifugal force per length acting on *dx* segment of the rotating axis changes its bending. The cross-section load corrections due to the centrifugal force are as follows:

- in-plane

$$p_{Y_\Omega}=\frac{d}{dx}\left(N\frac{dy}{dx}\right)-m(x)\omega^2 y, \tag{4}$$

- out-of-plane

$$p_{Z_\Omega}=\frac{d}{dx}\left(N\frac{dz}{dx}\right), \tag{5}$$

where

$N = \int_r^R m(x)\omega^2 x\,dx$ – the local centrifugal force at cross-section located at distance r from axis of the rotor shaft.

System of equations (1)÷(3) can be solved by applying Galerkin's method, where it is assumed that deflections of the elastic axis y, z, φ are equal to the sum of component deformations deriving from the considered eigen modes of the blade vibration:

$$y(x,t) = \sum_{j=1}^{J} \rho_j(t) y_j(x); \tag{6}$$

$$z(x,t) = \sum_{k=1}^{K} \delta_k(t) z_k(x); \tag{7}$$

$$\varphi(x,t) = \sum_{l=1}^{L} \eta_l(t) \varphi_l(x) \tag{8}$$

where

y_j, z_k, φ_l – eigen modes respectively bending in-plane, bending out-of-plane and torsion;
ρ_j, δ_k, η_l – time dependent shares of each eigen mode which are determined during computing process;
J, K, L – the numbers of considered bending and torsion eigen modes.

Using orthogonality condition for the eigen modes the equations of motion of axis (1)÷(3) can be converted into sets of equations (9)÷(11), where each equation concerns the oscillating motion of an equivalent structure of a single degree of freedom. The eigen mode frequency of this equivalent structure is equal the frequency of considered an eigen mode of the blade. Equations of motion of equivalent structures are as follows:

$$\ddot{\rho}_j + \rho_j p_j^2 = Q_{Y_j},\ j = 1,\ldots,\mathrm{J} \tag{9}$$

$$\ddot{\delta}_k + \delta_k f_k^2 = Q_{Z_k},\ k = 1,\ldots,\mathrm{K} \tag{10}$$

$$\ddot{\eta}_l + \eta_l \nu_l^2 = Q_{\varphi_l},\ l = 1,\ldots,\mathrm{L} \tag{11}$$

where

$Q_{Y_j}, Q_{Z_k}, Q_{\varphi_l}$ – generalized forces for considered eigen modes of the blade.

The equations of motion (9)÷(11) of equivalent masses of a single degree of freedom are solved by applying Runge-Kutta method. After determining at a given moment of time the contribution of generalized displacements ρ_j, δ_k, η_l, velocities and accelerations for each eigen mode the resultant parameters of the blade motion can be computed. Repeating the cycle of calculation allows to define deformation of blades and loads of rotor shaft.

The aerodynamic forces of blade segments at a given azimuth position on the rotor disk are calculated by using the blade element theory. The local angle of attack depends on temporary conditions of the cross-section airflow

$$\alpha = \varphi_g + \varphi - \mathrm{arctg}\left(\frac{v_Z}{v_X}\right), \tag{12}$$

where
φ_g – geometric twist,
v_Z, v_X – vertical and horizontal components of airflow,
φ – temporary pitch angle due to control and deformation.

Pitch angle of a blade element is determined as follows:

$$\varphi = \varphi_o + \varphi_x \cos \omega t + \varphi_y \sin \omega t + \varphi_{def} - \kappa\beta, \tag{13}$$

where
φ_o – blade collective control angle,
φ_x, φ_y – cyclic control angle due to roll and pitch deflection of the swashplate,
φ_{def} – angle of torsion deformation at given cross-section of blade,
κ – coefficient of coupling flapping and blade pitching,
β – temporary blade flapping angle at horizontal rotor head hinge.

RESULTS OF CALCULATIONS

The calculations were performed for data of a three-bladed rotor of a light helicopter with a take-off mass of 1,100 kg. The input data for a simulation program contains a set of eigen modes of the rotor blade. The frequencies of the considered modes are collected in Table 1.

Table 1. Frequencies of eigen modes of the blade [J. Stanisławski, 2014]

Eigen mode	F0	F1	F2	F3	C0	C1	T0	T1
Frequency related to ω = 49.65 [rd/s]	1.019	2.647	4.138	6.100	0.260	3.811	5.778	16.171

Symbols for eigen modes in Table 1 are as follows:
F – out-of-plane bending mode, C – in-plane bending mode, T – torsion mode,
digits after mode symbol are equal to the number of nodes.

The results of calculations include deformations and loads of blades and loads of the rotor shaft for the following states of flight:

- hover;
- level flight at high velocity (V = 180 km/h);
- autorotation at horizontal velocity V = 106 km/h and descent speed w = -7.9 m/s;
- pull-up maneuver for pulled-up collective lever mixed with pushed-over cyclic stick.

The parameters of rotor control in each state of flight are shown in Table 2.

Table 2. Parameters of rotor control [J. Stanisławski, 2014]

State of flight	Pitch of rotor shaft α_{shaft} [deg] 1)	Blade collective pitch φ_o [deg] 2)	Swashplate deflection in pitch channel $\varphi_{swash\text{-}y}$ [deg] 3)	Swashplate deflection in roll channel $\varphi_{swash\text{-}x}$ [deg] 4)
Hover	0	19.745	0	0
Level flight	-6.17	20.299	-4.797	-0.18
Autorotation	-3.02	12.271	-1.256	-0.085
Pull-up	15.0	19.840	-3.50	-5.0

1) α_{shaft} (+) for fuselage nose in up position
2) φ_o measured at blade root
3) $\varphi_{swash\text{-}y}$ (-) for cyclic stick pushover
4) $\varphi_{swash\text{-}x}$ (-) for cyclic stick deflection to ψ = 270° azimuth

The computations were executed for quasi-static conditions of the rotor control at a constant position of the swashplate and a pitch position of the rotor shaft during simulated phases of flight. The time of simulation comprises a period of ten rotor revolutions. The figures mainly present results for the last (the tenth) simulated revolution of the rotor. The rotation speed of the rotor was constant during simulations of flight states and was equal to $\omega = 49.65$ rd/s (100%), except autorotation case when the rotor speed was increased to $\omega = 54.61$ rd/s (110%). The pitch angle of the rotor shaft for each state of flight was defined by applying calculation of a helicopter balance based on a simplified model of a stiff rotor disk [3].

The results of computing the deformations and loads are presented as follows:

- plots of distribution of the blade deformation due to location of cross-section along the rotor radius at a characteristic azimuth position: $\psi = 0°$ over tail boom, $\psi = 90°$ for advancing blade, $\psi = 180°$ ahead position, $\psi = 270°$ for retreating blade (Fig. 2÷Fig. 7);
- plot of thrust and torsion moment of the rotor shaft in different states of flight (Fig. 8÷Fig. 10);
- maps of distribution of blade deformation and loads on the rotor disk, prepared by applying commercial Surfer 10 program [4]:

a) for hover (Fig. 11 and Fig. 12),
b) for level flight (Fig. 13÷Fig. 17),
c) for autorotation (Fig. 18÷Fig. 22),
d) for pull-up maneuver (Fig. 23÷Fig. 28).

In Fig. 8 is presented a simulation solution for full ten rotor revolutions where the torsion moment of the rotor shaft and forming it components from all three blades are shown. The influence of initial conditions vanishes about the sixth revolution of the rotor. Summing the shifted in phase components of all blades gives the resultant moment of the rotor shaft with a lesser amplitude compared to amplitude of component of each blade.

The variable conditions of the blade airflow involving changes of aerodynamic and inertial loads which generates the elastic deformations of the blades. For level flight in characteristic azimuth position the biggest torsion deformation of the blade can be observed for advancing blade at 90° azimuth (Fig. 2). In the case of pull-up maneuver (Fig. 6) the torsion deformation of the blade exceeds -2.7° with the nose of airfoil down. Smaller deformations of about -2° occur in autorotation flight. In hover condition at constant distribution of blade airflow with cyclic stick in a neutral position the elastic twist of the blade tip reaches value of -1.4°. For hover the map of blade torsion deformation on the rotor disk (Fig. 11) shows a circle shape of izolines.

The biggest values of the blade bending out-of-plane deflection are in pull-up maneuver (Fig. 7) in the zone of the advancing blade, where the blade tip rises over 0.5 m above the plane of rotation. For the retreating position the blade tip gets closer to the plane of rotation (Fig. 7 and Fig. 24) which is the result of a decreasing speed of airflow and an occurrence of flow separation zone at the blade tip.

The resultant load of rotor shaft depends on components of reaction of all blades (Fig. 8). The values of thrust and shaft moment for different states of flight are shown in Fig. 9 and Fig. 10. The largest moment driving rotor is in hover. A smaller value of shaft moment appears for a pull-up maneuver. In the considered quasi-static case, due to the position of the rotor shaft with a helicopter fuselage nose up, the greater part of the moment required to rotate the rotor comes from the airflow, where stream lines like in autorotation are directed from beneath to above rotation plane. In autorotation the negative value of shaft moment means that power absorbed from air flow allows to support and even to increase the rotation speed of the rotor. The lower mean value of rotor thrust in level flight compared to hover appears as the result of installing the small stub wings for a given version of a helicopter.

The distribution maps of deformations and loads of the blade on the rotor disk confirm generating the more complex conditions of airflow in forward flight state compared to circular distribution for hover (Fig. 11 and Fig. 12). In level flight at velocity V = 180 km/h for the advancing blade the attack angles reach at tip the negative values ($\alpha < -1.7°$) while for the retreating blade nearly approach critical value of airflow separation (Fig. 17). In autorotation due to small value of collective pitch the zone of negative angles of attack (Fig. 22) is wider comparing to level flight condition. In considered state of pull-up in region of the retreating blade appears the zone of separated flow at tip of blade (Fig. 28) what limits the increment of rotor thrust. In zone of advancing blade the angles of attack are positive (Fig. 27). The consequence of variable airflow and the dynamic effects due to cyclic control is generating the complex distributions of loads including blade torsion moments (Fig. 15, Fig. 20, Fig. 25) and bending moments (Fig. 16, Fig. 21, Fig. 26). Significant changes in distribution of blade out-of-plane bending moment in pull-up maneuver can be explained not only by an occurrence of separation zones but also by applying cyclic stick push-over which causes large pitch motion of the blade (±8.5°) and pulsation of the bending moment in cross-sections located at 0.5 R÷0.8 R of the rotor radius.

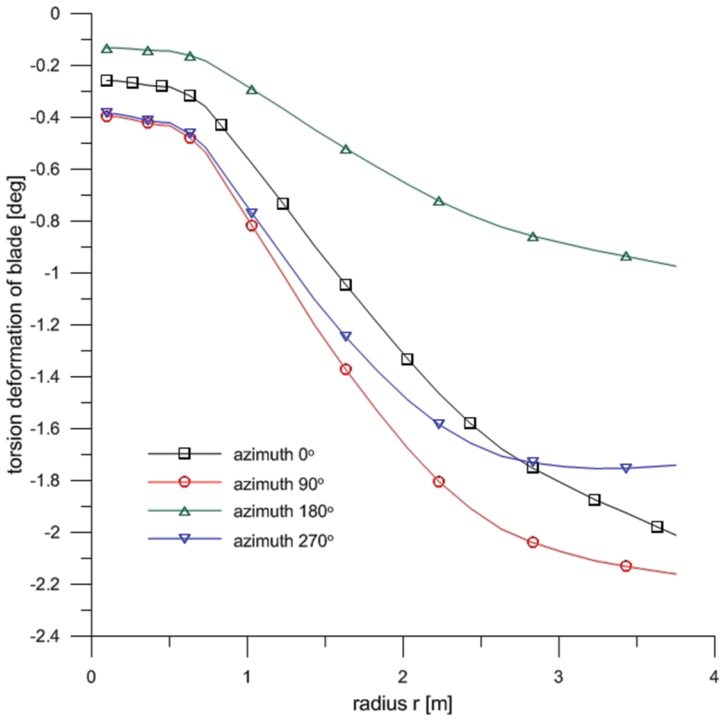

Fig. 2. Distribution of torsion deformation of blade due to radius and azimuth position, level flight at velocity V = 180 km/h, ISA condition at sea level [J. Stanisławski, 2014]

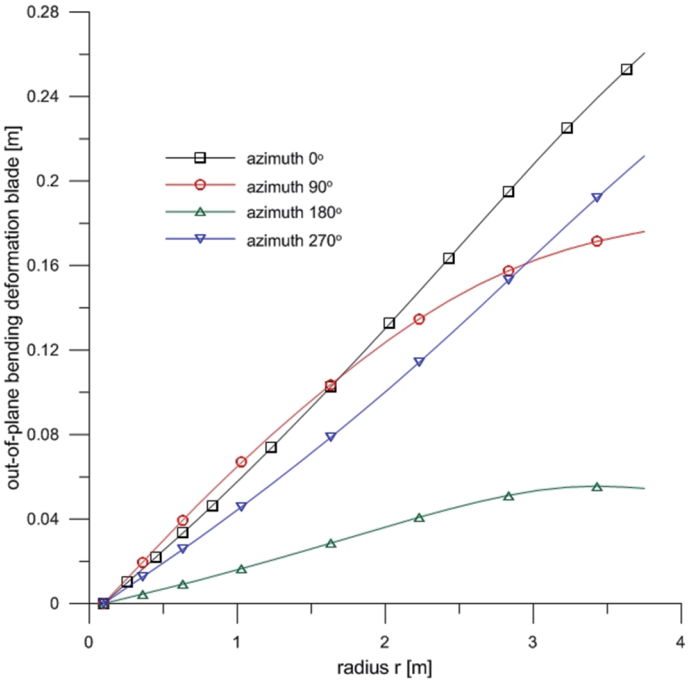

Fig. 3. Distribution of out-of-plane bending deformation of blade due to radius and azimuth position, level flight at velocity V = 180 km/h, ISA condition at sea level [J. Stanisławski, 2014]

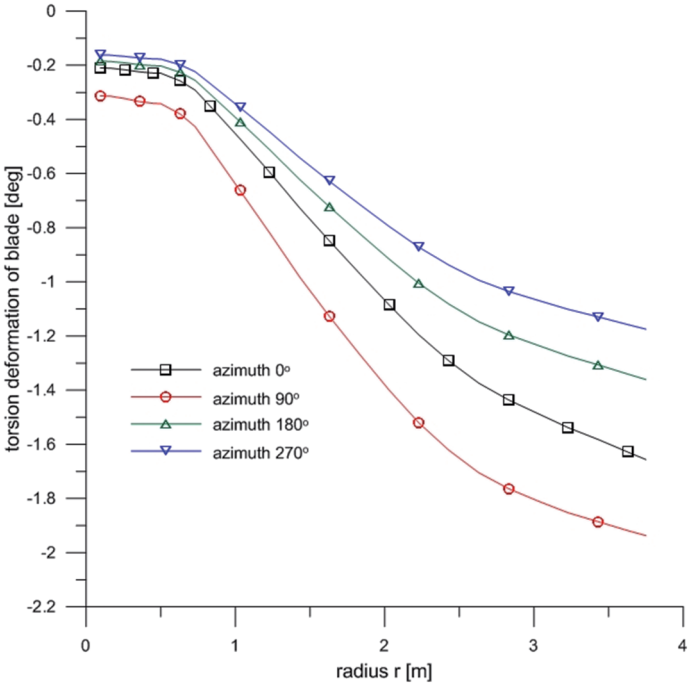

Fig. 4. Distribution of blade torsion deformation due to radius and azimuth position, in autorotation at horizontal velocity of flight V = 106 km/h and descent w = -7.9 m/s; ISA condition at sea level [J. Stanisławski, 2014]

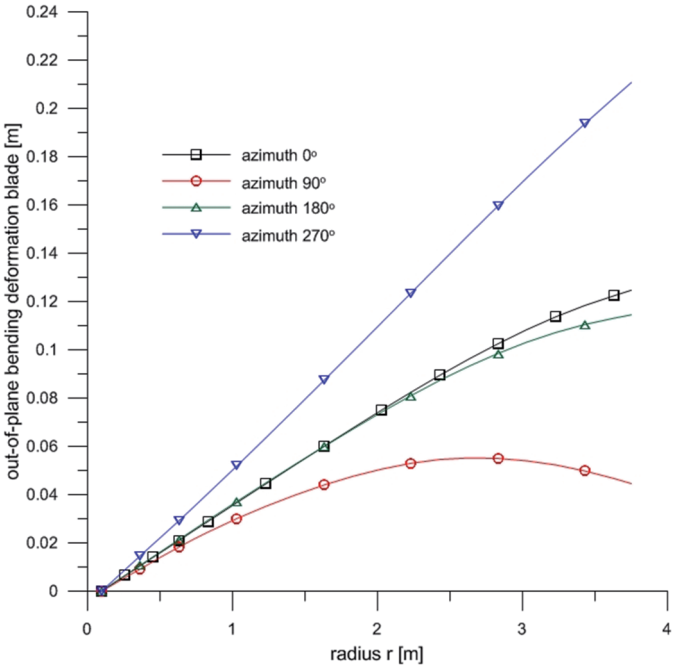

Fig. 5. Distribution of out-of-plane bending deformation of blade due to radius and azimuth position, autorotation at horizontal velocity of flight V = 106 km/h and descent speed w = -7.9 m/s; ISA condition at sea level [J. Stanisławski, 2014]

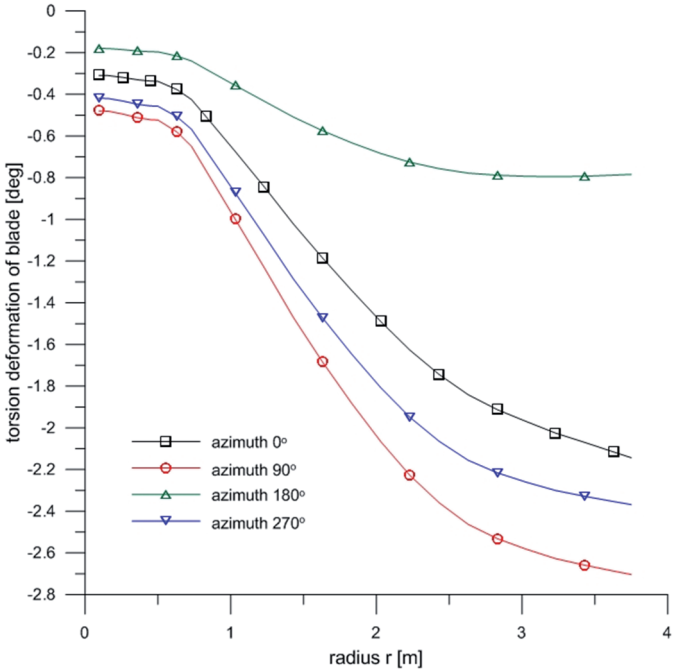

Fig. 6. Distribution of torsion deformation of blade due to radius and azimuth position, quasi-static state of pull-up maneuver at velocity of flight V = 100 km/h, ISA condition at sea level [J. Stanisławski, 2014]

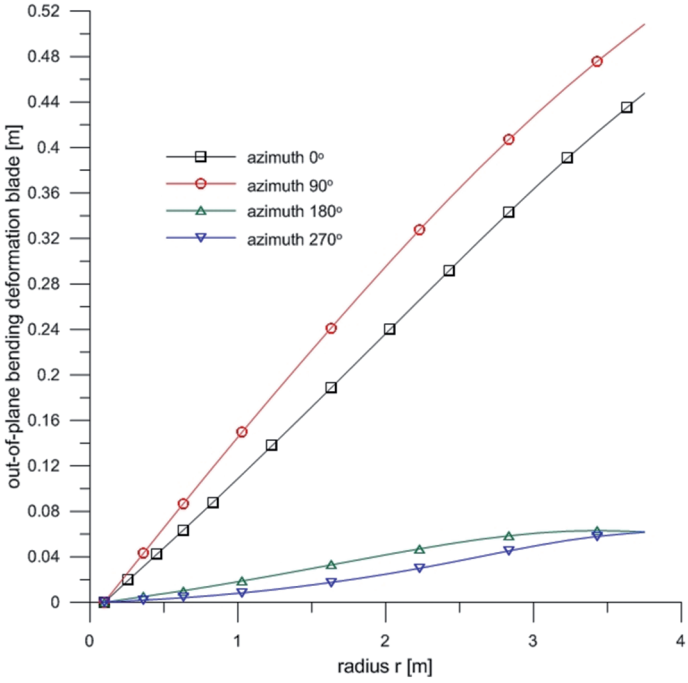

Fig. 7. Distribution of out-of-plane bending deformation of blade due to radius and azimuth position, quasi-static state of pull-up maneuver, at velocity of flight V = 100 km/h, ISA condition at sea level [J. Stanisławski, 2014]

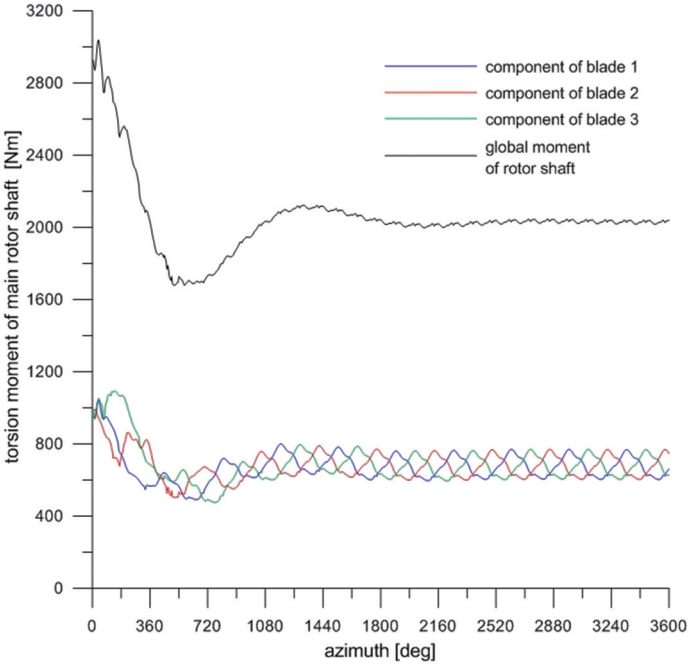

Fig. 8. Torsion moment of rotor shaft, horizontal flight V = 180 km/h at sea level, ISA condition [J. Stanisławski, 2014]

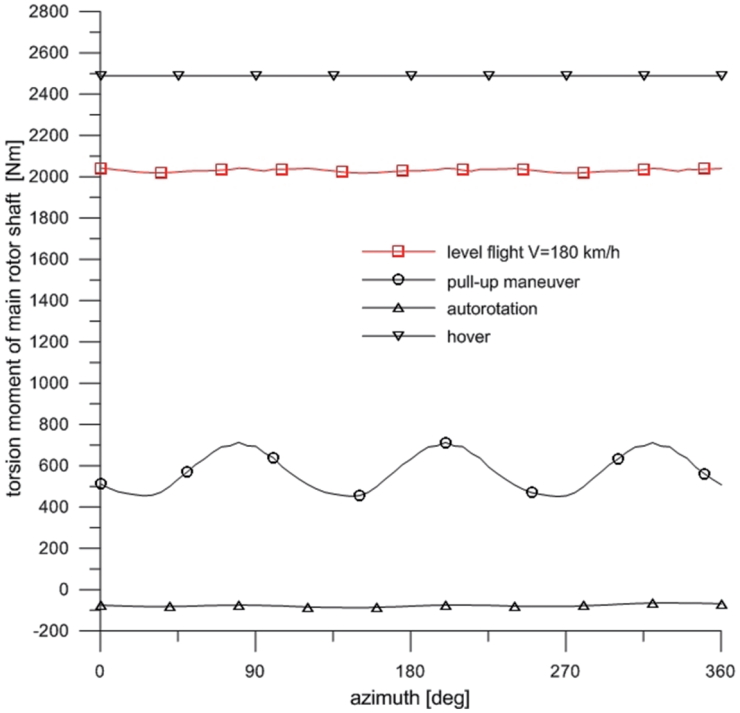

Fig. 9. Torsion moment of rotor shaft for different states of flight [J. Stanisławski, 2014]

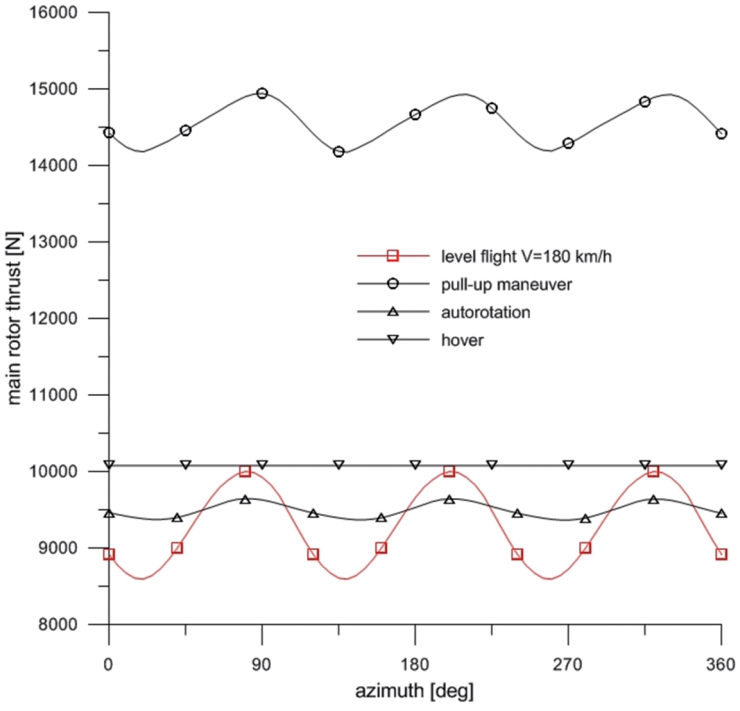

Fig. 10. Thrust of main rotor for different states of flight [J. Stanisławski, 2014]

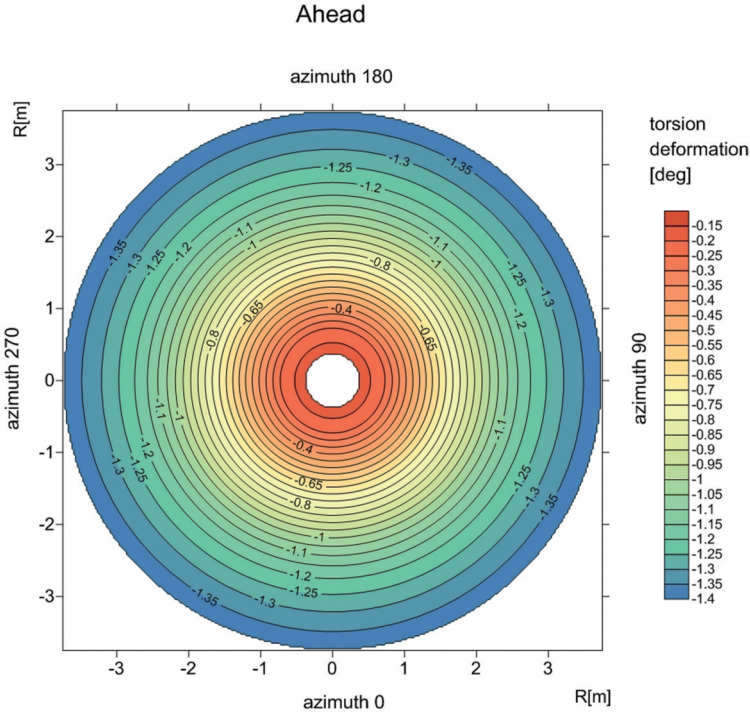

Fig. 11. Distribution of blade torsion deformation on rotor disk in hover [J. Stanisławski, 2014]

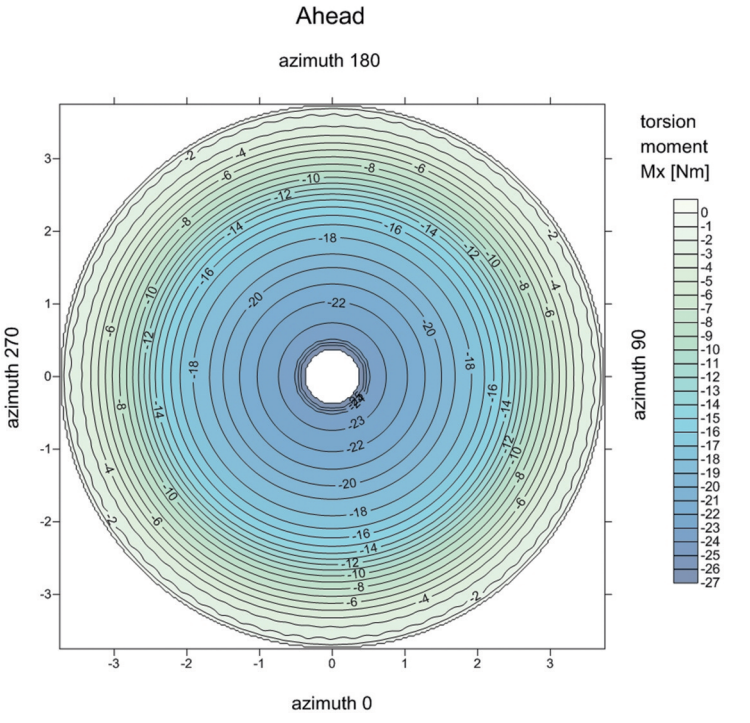

Fig. 12. Distribution of blade torsion moment at rotor disk in hover [J. Stanisławski, 2014]

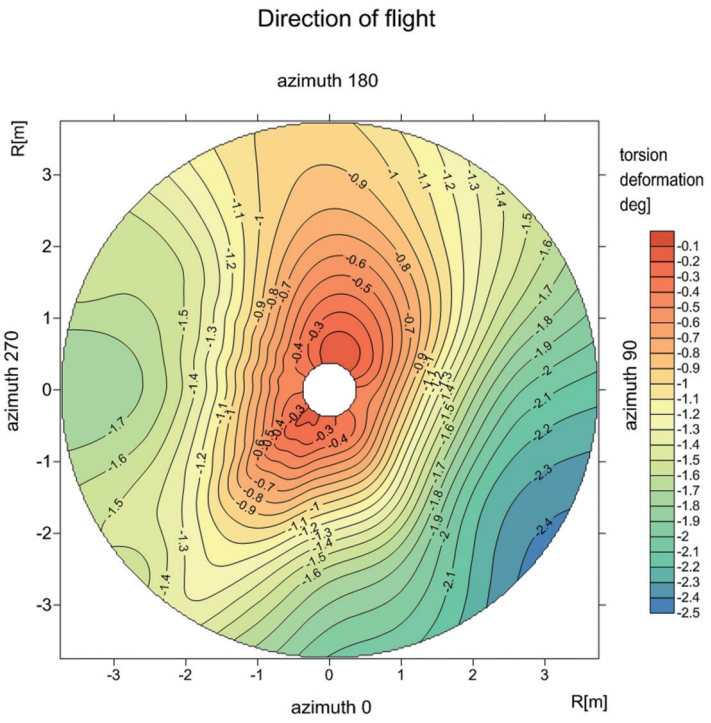

Fig. 13. Distribution of blade torsion deformation on rotor disk in level flight V = 180 km/h [J. Stanisławski, 2014]

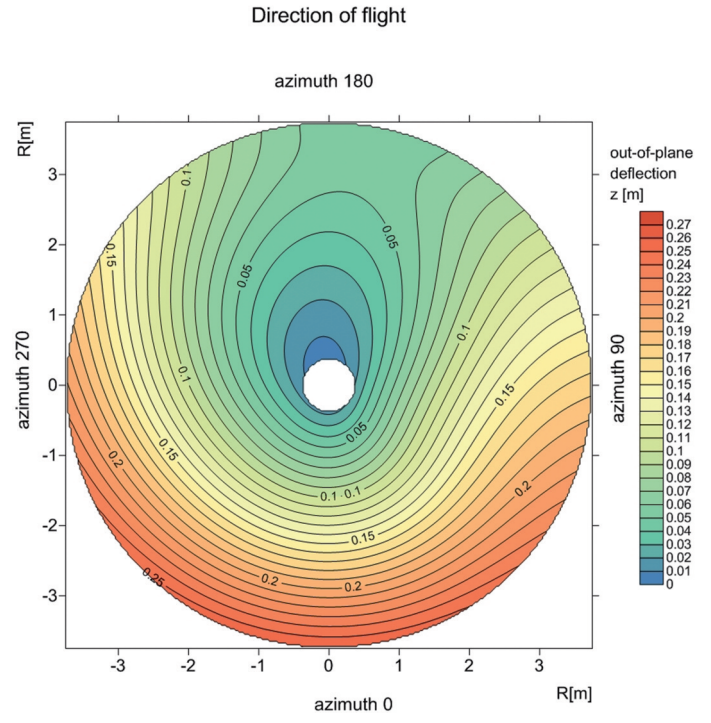

Fig. 14. Rotor disk distribution of out-of-plane blade deflection in level flight V = 180 km/h [J. Stanisławski, 2014]

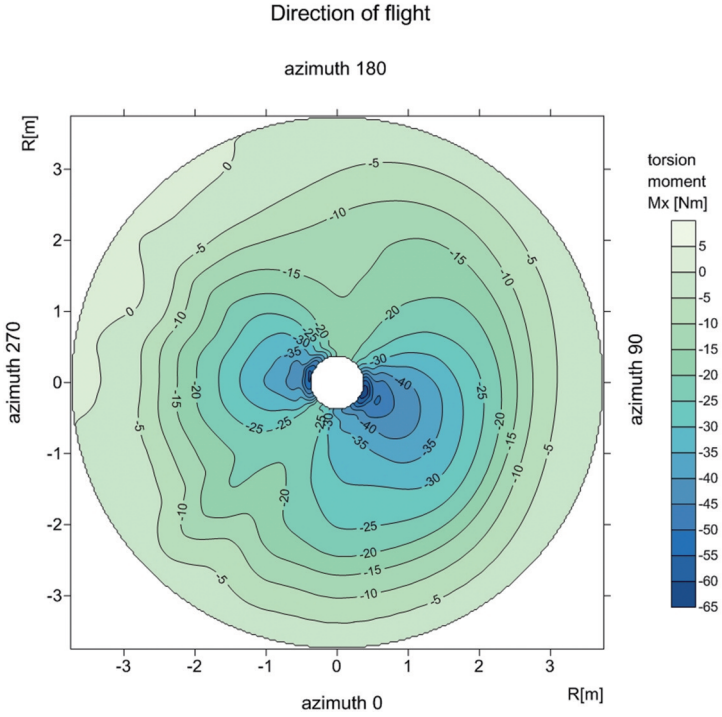

Fig. 15. Distribution of blade torsion moment on rotor disk in level flight V = 180 km/h [J. Stanisławski, 2014]

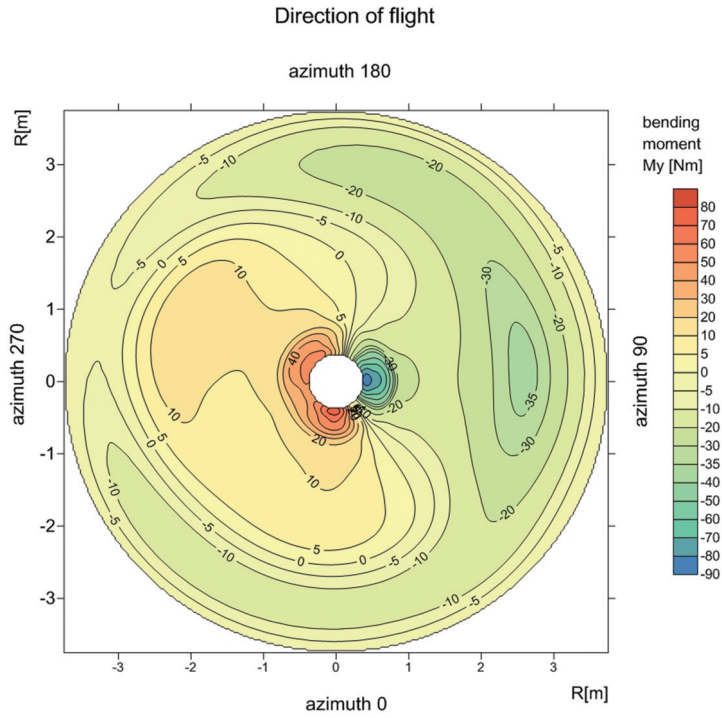

Fig. 16. Rotor disk distribution of out-of-plane blade bending moment in level flight V = 180 km/h [J. Stanisławski, 2014]

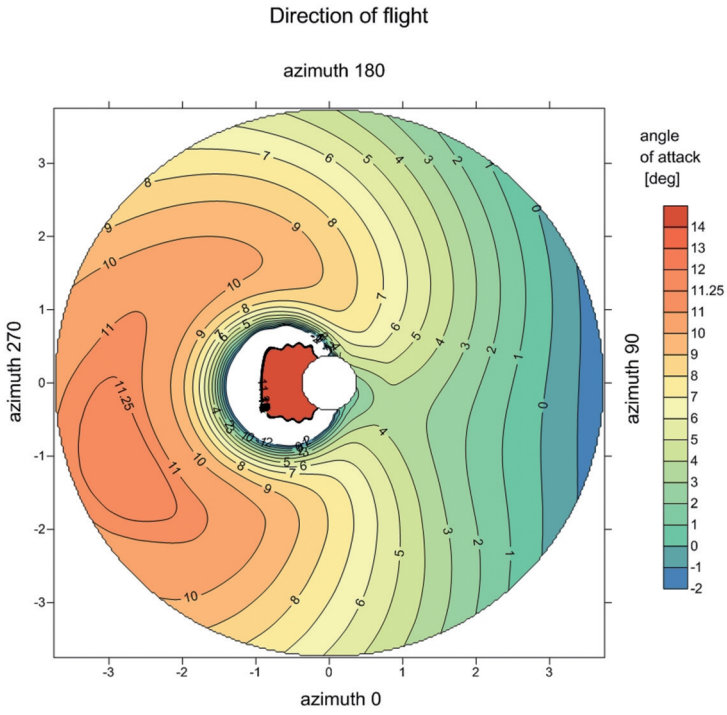

Fig. 17. Rotor disk distribution of attack angle of blade cross-sections in level flight V = 180 km/h [J. Stanisławski, 2014]

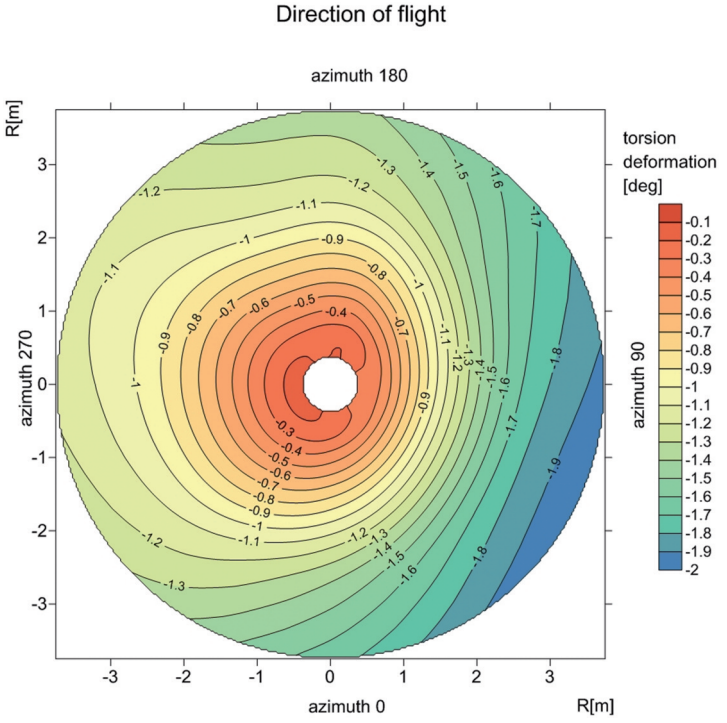

Fig. 18. Distribution of blade torsion deformation on rotor disk in autorotation [J. Stanisławski, 2014]

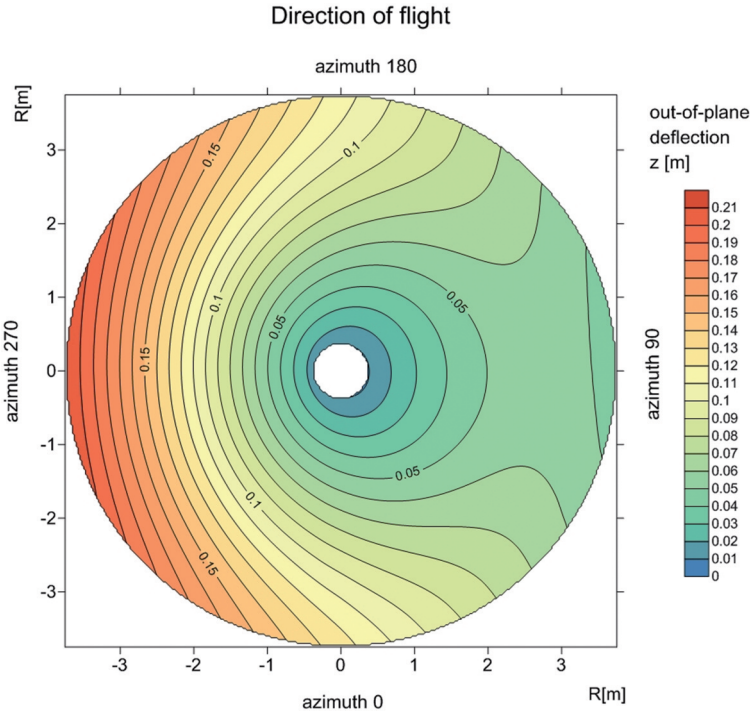

Fig. 19. Rotor disk distribution of out-of-plane deflection in autorotation [J. Stanisławski, 2014]

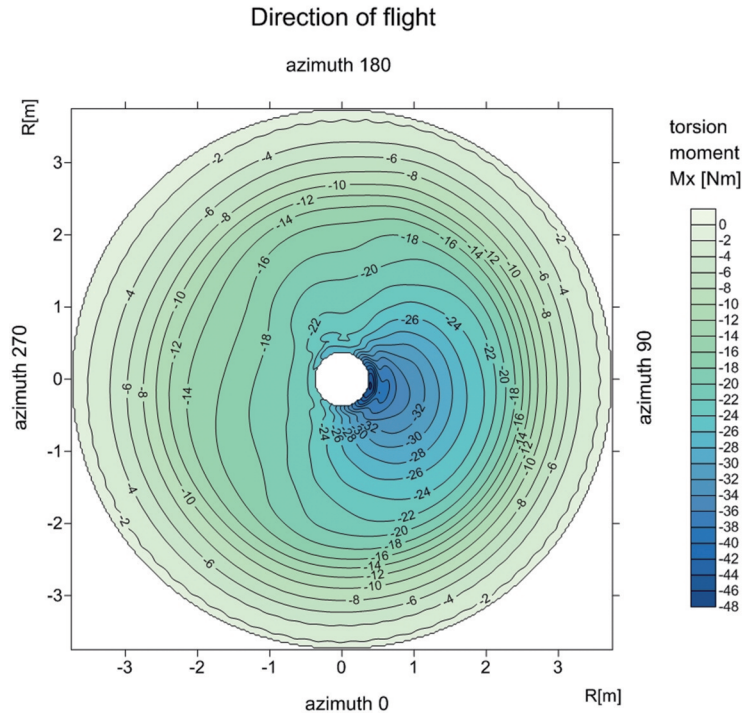

Fig. 20. Rotor disk distribution of blade torsion moment in autorotation [J. Stanisławski, 2014]

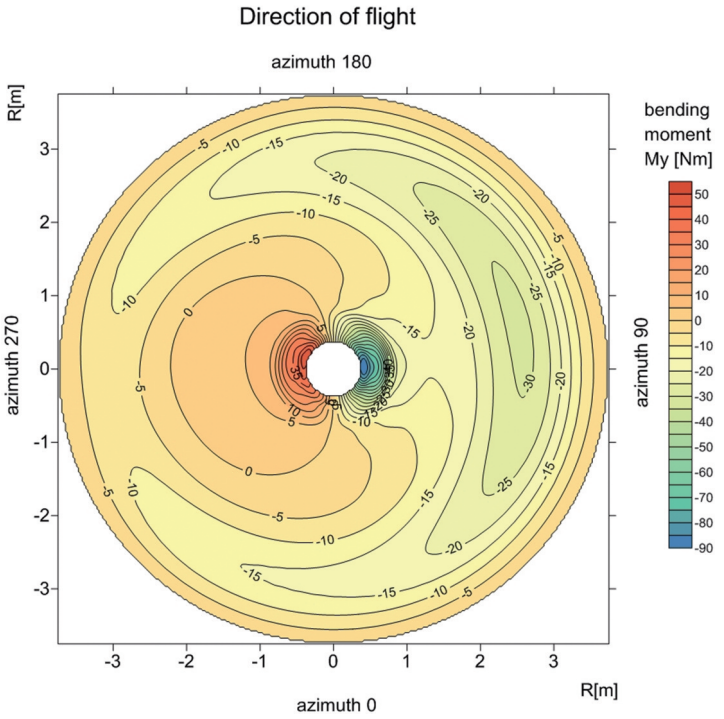

Fig. 21. Rotor disk distribution of out-of-plane blade bending moment in autorotation [J. Stanisławski, 2014]

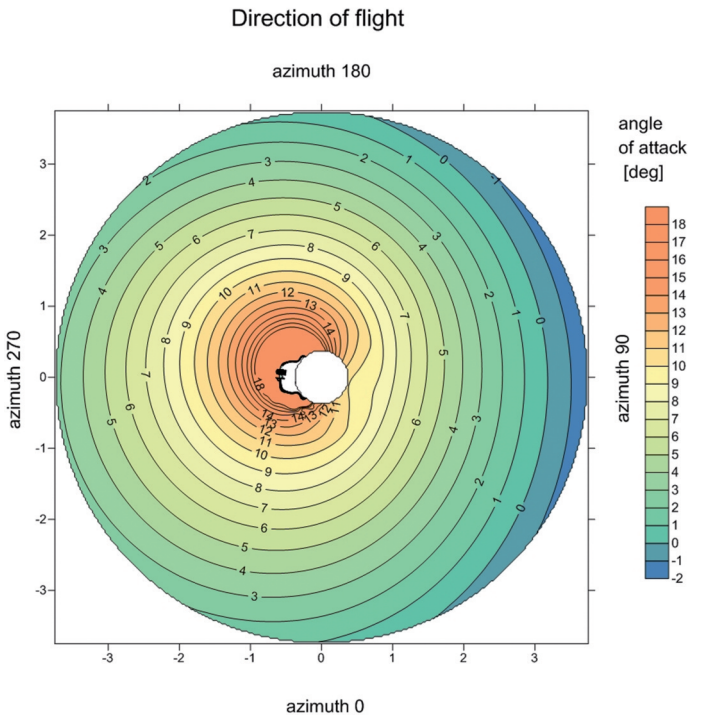

Fig. 22. Rotor disk distribution of attack angle of blade cross-sections in autorotation [J. Stanisławski, 2014]

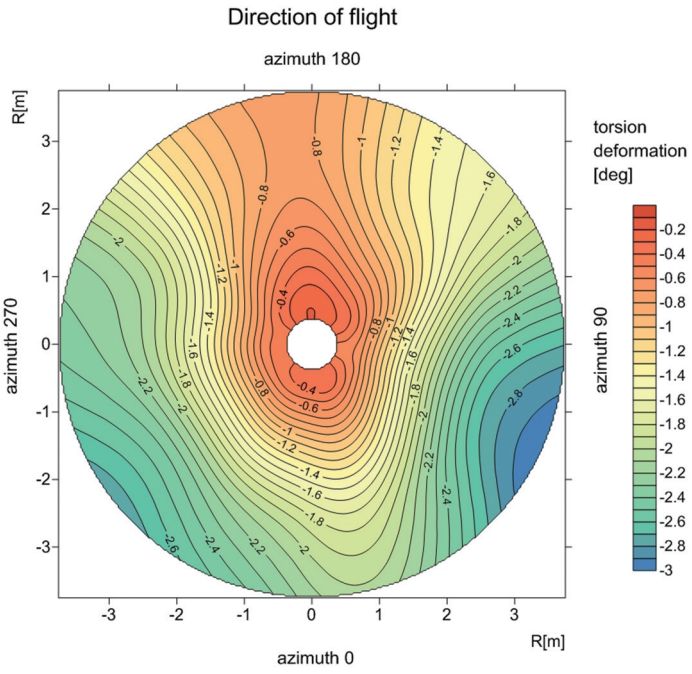

Fig. 23. Rotor disk distribution of blade torsion deformation in quasi-static state of pull up maneuver [J. Stanisławski, 2014]

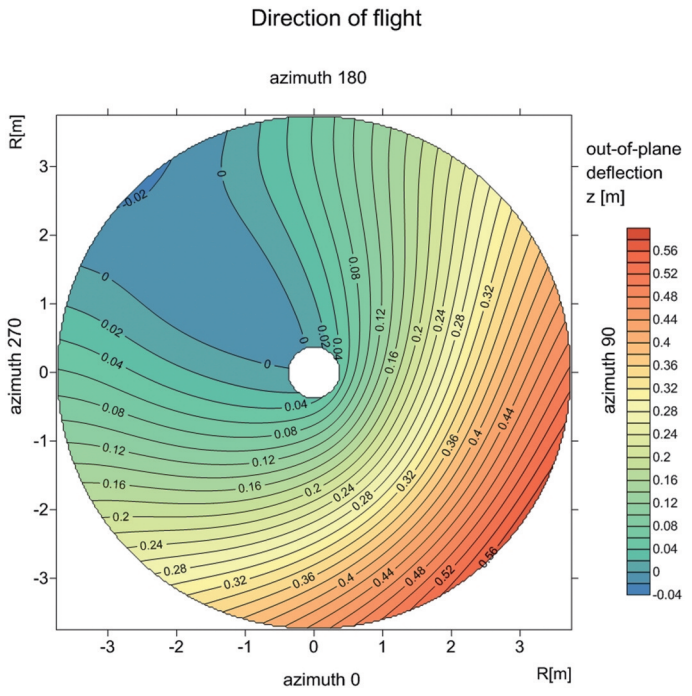

Fig. 24. Rotor disk distribution of out-of-plane blade deflection in quasi-static state of pull up maneuver [J. Stanisławski, 2014]

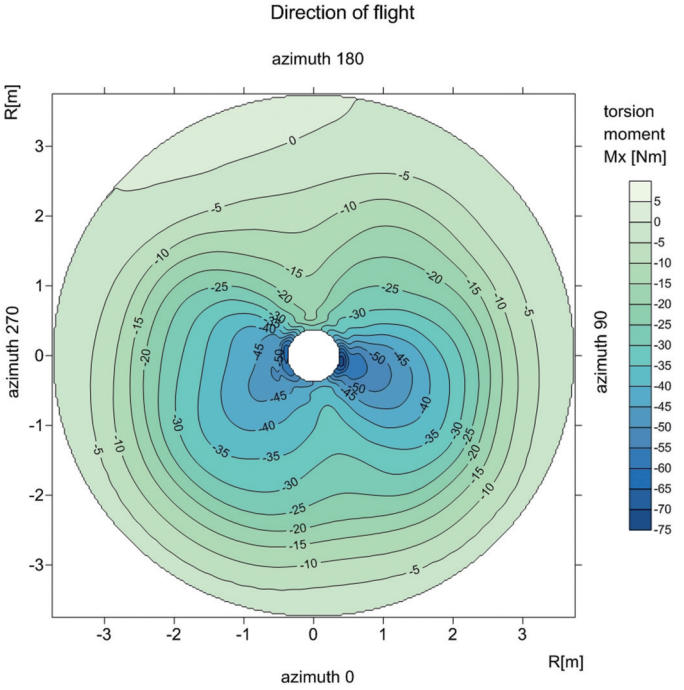

Fig. 25. Rotor disk distribution of blade torsion moment in quasi-static state of pull up maneuver [J. Stanisławski, 2014]

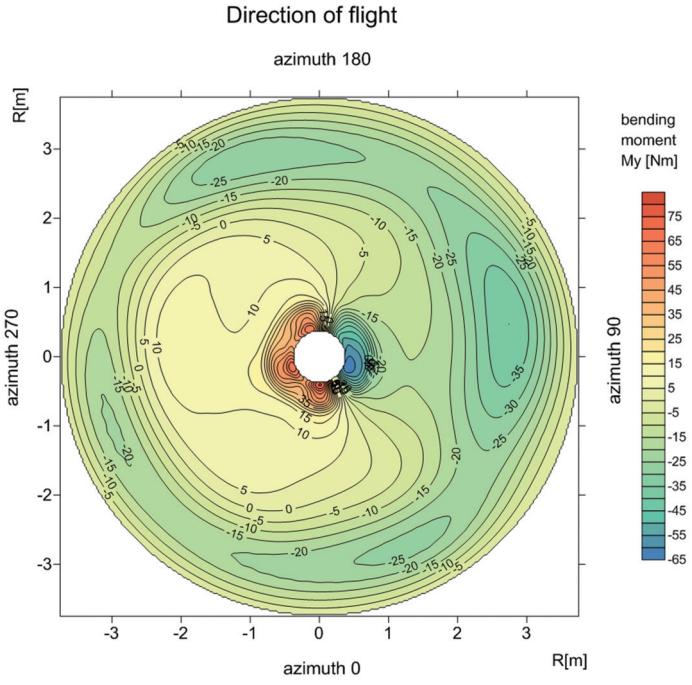

Fig. 26. Rotor disk distribution of out-of-plane blade bending moment in quasi-static state of pull up maneuver [J. Stanisławski, 2014]

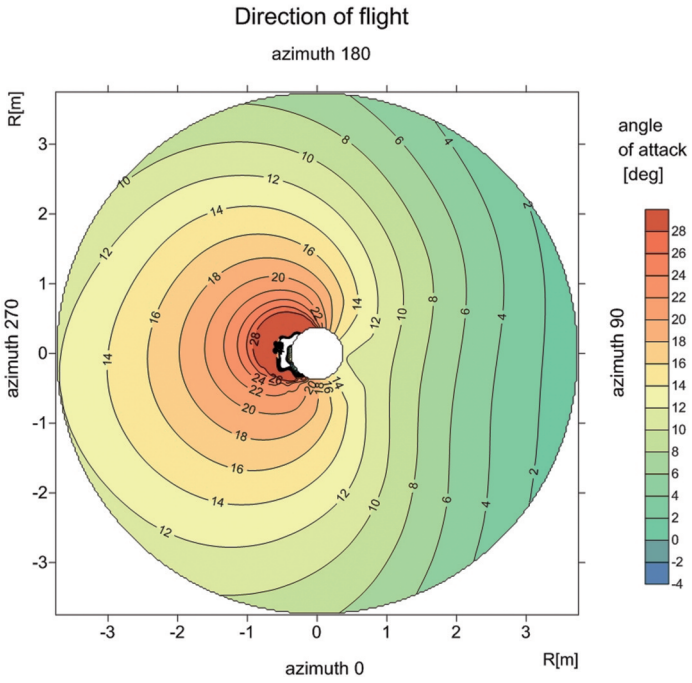

Fig. 27. Rotor disk distribution of attack angle of blade cross-sections in quasi-static state of pull up maneuver [J. Stanisławski, 2014]

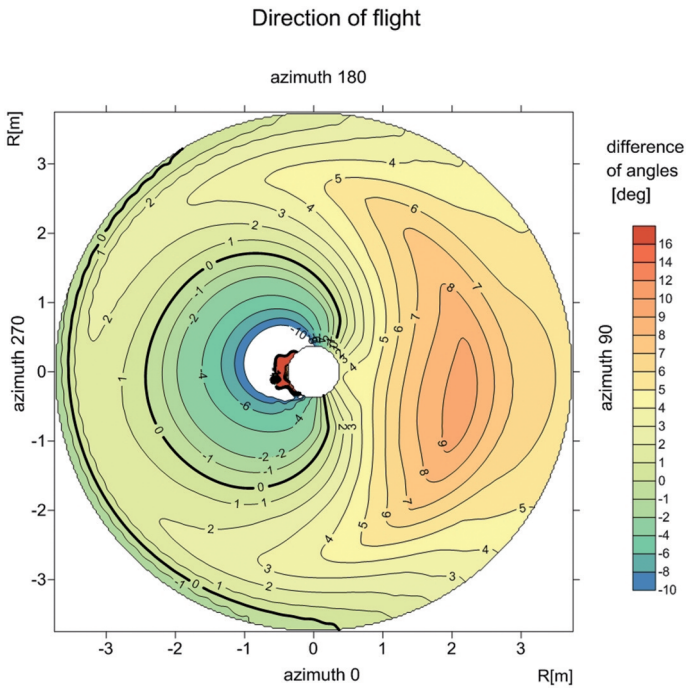

Fig. 28. Rotor disk distribution of difference of critical and local attack angles of blade cross-sections in quasi-static state of pull up maneuver [J. Stanisławski, 2014]

CONCLUSIONS

The performed calculations allow for defining the range of change of operating parameters for the helicopter main rotor in characteristic states of flight. The results of the simulation give useful data to create a spectrum of variable loads generated by the rotor. The developed program can be applied to predict limits of a helicopter flight envelope and to avoid potentially dangerous conditions of flight.

REFERENCES

[1] Stanisławski, J. (2008). Obliczenia w wybranych stanach lotu parametrów pracy czterołopatowego wirnika nośnego śmigłowca PZL Sokół z profilami NACA, Institute of Aviation, internal report GR/00011/BP/2008, Warszawa, (in Polish).
[2] Stanisławski, J. (2009). Wirnik nośny śmigłowca z indywidualnym sterowaniem katem nastawienia łopat w warunkach lotu ustalonego, Institute of Aviation, internal report 00034/BP/2008, Warszawa, (in Polish).
[3] Stanisławski, J. (2004). Instrukcje użytkowania programów komputerowych dotyczących zagadnień mechaniki lotu śmigłowca i obciążeń łopat wirnika nośnego, Institute of Aviation, internal report GR/01/BP/2004, Warszawa, (in Polish).
[4] Galon, Z. (2011). *Surfer 10. Podręcznik użytkownika*, (user manual in Polish), Gambit Centrum Oprogramowania i Szkoleń, Kraków.

OBRAZ OBCIĄŻEŃ I ODKSZTAŁCEŃ ŁOPATY WIRNIKA NOŚNEGO ŚMIGŁOWCA W WYBRANYCH STANACH LOTU

Streszczenie

Praca obejmuje określenie poziomu zmian obciążeń wirnika nośnego i odkształceń łopat występujących w różnych warunkach lotu możliwych do wystąpienia w granicach obwiedni stanów lotu śmigłowca: zawis, lot poziomy, autorotacja, wyrwanie. Wartości obciążeń elementów wirnika wyznaczono symulacyjnie z zastosowaniem programu komputerowego uwzględniającego model odkształcalnej łopaty. Do rozwiązania równań ruchu łopat wykorzystano metodę Galerkina. Wyniki obliczeń przedstawiono w formie wykresów pokazujących rozkłady obciążeń i odkształceń.

Słowa kluczowe: śmigłowiec, wirnik, łopata.